

Article

# Study on Line-Start Permanent Magnet Assistance Synchronous Reluctance Motor for Improving Efficiency and Power Factor

Hyunwoo Kim <sup>1</sup> , Yeji Park <sup>1</sup>, Huai-Cong Liu <sup>2</sup>, Pil-Wan Han <sup>3</sup> and Ju Lee <sup>1,\*</sup>

<sup>1</sup> Department of Electrical Engineering, Hanyang University, Seoul 04763, Korea; khw7481@hanyang.ac.kr (H.K.); yejipark@hanyang.ac.kr (Y.P.)

<sup>2</sup> Hyundai Transys, Hwaseong 18280, Korea; hcliu@hyundai-transys.com

<sup>3</sup> Electric Machines and Drives Research Center, Korea Electrotechnology Research Institute, Changwon 51543, Korea; pwhan@keri.re.kr

\* Correspondence: julee@hanyang.ac.kr; Tel.: +82-2220-0342

Received: 12 December 2019; Accepted: 9 January 2020; Published: 13 January 2020



**Abstract:** In order to improve the efficiency, a line-start synchronous reluctance motor (LS-SynRM) is studied as an alternative to an induction motor (IM). However, because of the saliency characteristic of SynRM, LS-SynRM have a limited power factor. Therefore, to improve the efficiency and power factor of electric motors, we propose a line-start permanent magnet assistance synchronous reluctance motor (LS-PMA-SynRM) with permanent magnets inserted into LS-SynRM. IM and LS-SynRM are selected as reference models, whose performances are analyzed and compared with that of LS-PMA-SynRM using a finite element analysis. The performance of LS-PMA-SynRM is analyzed considering the position and length of its permanent magnet, as well as its manufacture. The final model of LS-PMA-SynRM is designed for improving the efficiency and power factor of electric motors compared with LS-SynRM. To verify the finite element analysis (FEA) result, the final model is manufactured, experiments are conducted, and the performance of LS-PMA-SynRM is verified.

**Keywords:** efficiency; finite element analysis; line-start synchronous reluctance motor; permanent magnet; power factor

## 1. Introduction

As the electrical machine industry is developing, electric energy consumption has been increasing. In industrial applications, electric motors account for energy consumption between 35% and 40% [1–3]. If the efficiency of the electric motor is low, environmental problems such as emission of greenhouse gases are induced. Electrical motors are not a unique problem regarding energy consumption and efficiency. There are also more complex systems such as modern data centers, where there are a lot of electrical motors (and highly energy consumption), because of environment control, cooling, air ventilating, and so on [4,5]. In order to solve these environmental problems, the minimum energy performance standards (MEPS) are enacted by regulating motor efficiency. According to MEPS, the energy efficiency of industrial motors is standardized by power range (0.75–150 kW), and efficiency classes are defined from IE1 to IE4. Recently, the industrial motors have been required to satisfy the IE4 class efficiency according to the strength of MEPS [6].

Induction motors (IMs) account for 70% of industrial motors because of their simple structure and low manufacture cost [1–3]. However, IMs have the secondary copper loss that limits the improvement in their efficiency [7–10]. Therefore, to replace IMs, new types of motor are being studied to improve the efficiency such as line-start synchronous reluctance motors (LS-SynRMs). As LS-SynRMs are operated at a synchronous speed, they do not exhibit secondary copper loss [9,10]. Furthermore, unlike

the synchronous motor, this machine does not require an inverter to reach the synchronous speed. Therefore, because the inverter is not necessary, the system cost of these machines is lower compared with synchronous motors and efficiency of LS-SynRMs is better compared with IMs [11–13]. Therefore, LS-SynRM has received attention as a better alternative to IM as an industrial motor [14,15].

The characteristics of LS-SynRM are the same as those of SynRM. Therefore, LS-SynRMs can improve the efficiency of electric motors; however, the power factor is reduced compared with that of IMs because the saliency characteristic [16–18]. However, for the industrial machines, the power factor is also an important factor because the reactive power is affected by the generated power of a generator; further, power factor affects electrical cost [19]. Therefore, according to IEC 60034-1, there is a specification for the power factor of the industrial motor. The permanent magnet synchronous reluctance motor (PMA-SynRMs) with ferrite magnet inserted into SynRM has higher efficiency and power factor compared with SynRMs [20,21]. Therefore, we proposed a line start permanent magnet assistance synchronous reluctance motor (LS-PMA-SynRM) for improving the efficiency and power factor of LS-SynRMs [22,23].

When designing an electrical machine, a magnetic equivalent circuit (MEC) or a finite element analysis (FEA) is used [24–31]. MEC is constructed using the magnetic resistance and magneto motive force considering the magnetic flux paths. By applying a circuit theory, the equation of MEC is solved and the magnetic flux density is simply calculated. However, in a complex rotor structure such as SynRM, it is difficult to analyze the motor because MEC is not easy to construct [30]. On the other hand, in FEA, the solution region is discretized into finite elements using mesh generators and the solution of the governing equation for each element is solved using numerical method [32]. As the solution is based on the element, FEA can be applied to various electrical machine structures [28–31]. Therefore, FEA is powerful numerical method to analyze LS-PMA-SynRM having the complex rotor structure.

In this study, the characteristics of LS-PMA-SynRM are analyzed to improve the efficiency and power factor using FEA. Based on the mathematical model, the characteristics of LS-SynRM and LS-PMA-SynRM are compared. Furthermore, the power factor is analyzed according to the magnetic flux of the permanent magnet. To compare the characteristics of LS-PMA-SynRM, a 5.5 kW IM and LS-SynRM are selected as the reference models. The LS-PMA-SynRM is designed based on the LS-SynRM. The characteristics of LS-PMA-SyRM are then analyzed considering the position and length of the permanent magnet. The final model is designed to maximize the efficiency and power factor. To verify the FEA result, the final model is manufactured and tested for the characteristics of LS-PMA-SynRM.

This paper is organized as follows. In Section 2, the characteristics of LS-SynRM and LS-PMA-SynRM are discussed with respect to the efficiency and power factor. In Section 3, the characteristics of the reference models (IM and LS-SynRM) are analyzed and compared. In Section 4, the performance of LS-PMA-SynRM is analyzed considering the position and length of the permanent magnet. In Section 5, to verify the FEA result, experiments are conducted, and the results obtained for IM and LS-PMA-SynRM are compared. Finally, Section 5 presents the conclusion.

## 2. Characteristics of LS-SynRM and LS-PMA-SynRM

The operating principle of LS-machines is classified into asynchronous and synchronous speed. Therefore, the subsections are discussed with the characteristic of LS-machines according to the operating speed. In Section 2.1, the principle of LS-machines is discussed at asynchronous speed. In Section 2.2, the main performances, such as efficiency and power factor, are determined at synchronous speed.

### 2.1. Asynchronous Operation

In asynchronous speed, the rotor current is generated by the slip speed that is the relative speed between the synchronous speed and the rotor speed. Similar to the operation principle of IMs, the

rotor current provides the required magnetic torque for the speed to approach synchronous speed. This magnetic torque is expressed as follows and is the same for IMs [33]:

$$T_c = K_T \Phi_m I_2 \cos \phi, \quad (1)$$

where  $T_c$  is the torque generated by squirrel-cage bar,  $K_T$  is the torque constant,  $\Phi_m$  is the mutual flux,  $I_2$  is rotor current, and  $\phi$  is the power factor angle.

## 2.2. Synchronous Operation

### 2.2.1. Efficiency

In synchronous speed, the operation principle of LS-machines is the same as that for synchronous machines. The efficiency of the synchronous machines is determined based on the mechanical power of motor, core loss, and copper loss as follows:

$$\eta = \frac{P_{out}}{P_{in}} = \frac{P_{out}}{P_{out} + P_{loss}} = \frac{T_e \omega_e}{T_e \omega_e + P_{copper} + P_{core}}, \quad (2)$$

where  $\eta$  is efficiency,  $P_{out}$  is mechanical power,  $P_{in}$  is electrical input power,  $P_{loss}$  is total loss of motor,  $T_e$  is torque of motor,  $\omega_e$  is synchronous speed,  $P_{copper}$  is copper loss, and  $P_{core}$  is core loss.

Equation (2) indicates that if the power is the same, the efficiency is determined by the losses of LS machines. The main losses of LS machines are classified into core loss and copper loss. The core loss is dependent on the magnetic flux density of the core and frequency. However, the magnetic flux density of the core is determined when the motor is designed, and the frequency is determined by the synchronous speed of LS machines. Therefore, there is a limitation when reducing core loss. In contrast, the copper loss is dependent on the resistance and current. If the torque per current is increased, the copper loss is reduced, and the efficiency can be increased. Therefore, the design method for improving the torque per current is important to improve the efficiency.

When comparing LS-SynRMs and LS-PMA-SynRMs, the LS-PMA-SynRMs generate the additional magnetic torque. Therefore, because the torque per current of LS-PMA-SynRM is larger than LS-SynRM, the efficiency of LS-PMA-SynRM can be improved. The torque of LS-PMA-SynRM is as follows:

$$T_e = \frac{3P}{2} [\lambda_a i_q + (L_d - L_q) i_d i_q], \quad (3)$$

where  $T_e$  is torque of motor,  $P$  is pole,  $\lambda_a$  is the flux linkage,  $i_d$  and  $i_q$  are  $dq$ -axis current, and  $L_d$  and  $L_q$  are  $dq$ -axis inductance.

### 2.2.2. Power Factor

The power factor is determined by the phase angle difference between the voltage and the current. This phase angle difference can be determined from the  $dq$ -axis vector diagram. Figure 1a,c,e shows the structure of an interior permanent magnet synchronous motor (IPMSM), LS-SynRM, and LS-PMA-SynRM to define the  $dq$ -axis vector diagram. In general, because the  $d$ -axis is defined as the main flux axis, the  $d$ -axis of IPMSM is the magnetizing direction of a permanent magnet and the  $d$ -axis of the LS-SynRM is a segment through which the main magnetic flux passes. In the case of LS-PMA-SynRM, the  $d$ -axis can be defined as the segment because the permanent magnet inserted into LS-SynRM is only used as the assistant torque. Therefore, in Figure 1e, the magnetic flux of the permanent magnet is generated along the  $q$ -axis. Figure 1b,d,f shows the vector diagram of IPMSM, LS-SynRM, and LS-PMA-SynRM. The magnetic flux of the permanent magnet is the  $d$ -axis in Figure 1b. In contrast, the magnetic flux of the permanent magnet is negative along the  $q$ -axis in Figure 1f because the path of main flux is segments.

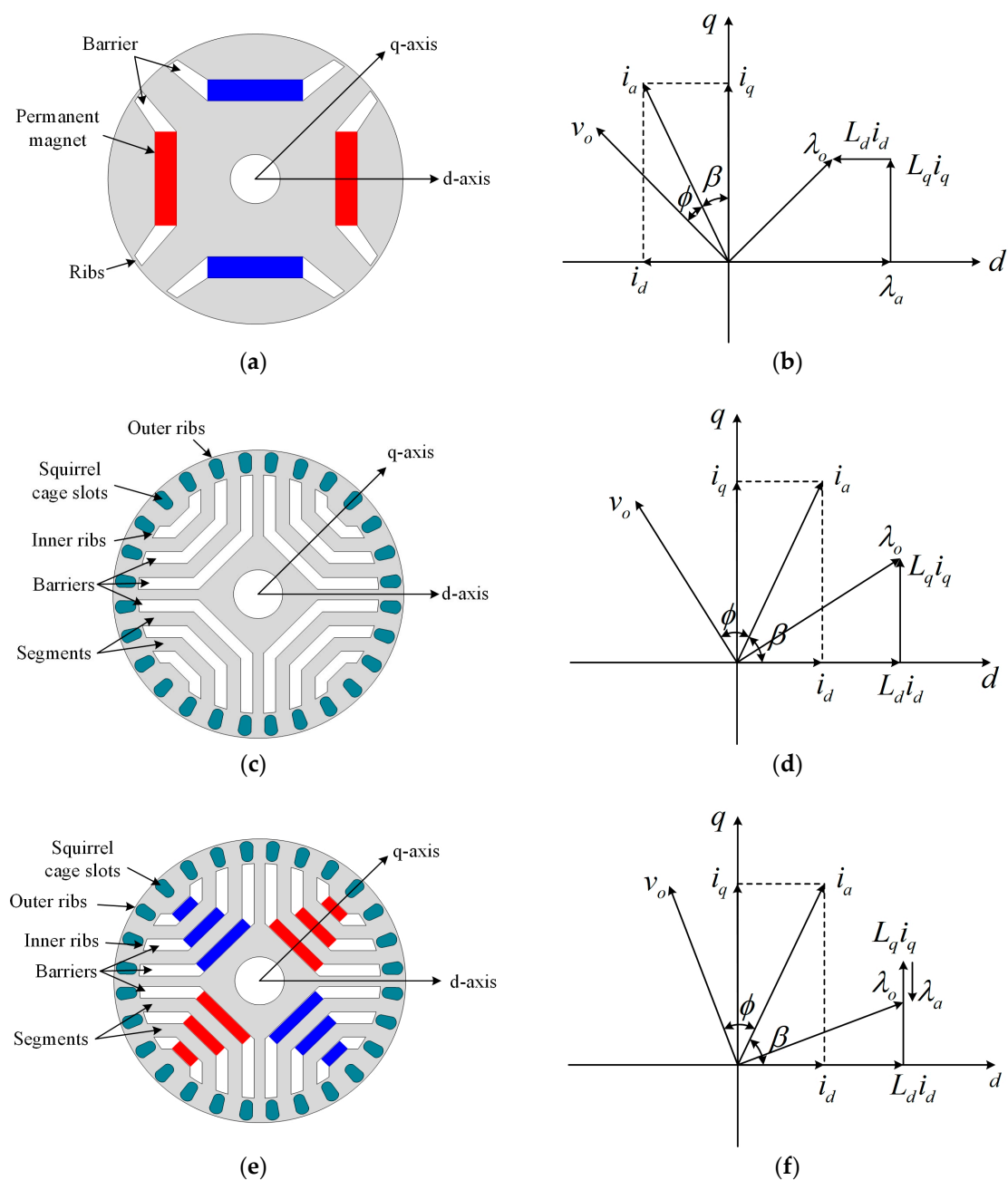


**Figure 1.** Structure of a line-start synchronous reluctance motor (LS-SynRM) and vector diagram (a) structure of an interior permanent magnet synchronous motor (IPMSM) (b) vector diagram of an IPMSM, (c) structure of a LS-SynRM, (d) vector diagram of a LS-SynRM, (e) structure of a line-start permanent magnet assistance synchronous reluctance motor (LS-PMA-SynRM), (f) vector diagram of a LS-PMA-SynRM.

LS-PMA-SynRMs with ferrite permanent magnet inserted into SynRM have the flux linkage owing to the permanent magnet. This flux linkage is affected by the vector diagram and the power factor is also affected. Figure 2 shows the vector diagram of LS-PMA-SynRM according to flux linkage owing to the permanent magnet ( $\lambda_a$ ). In Figure 2, the difference between the voltage and the current phase is decreased according to the increasing flux linkage. Therefore, the larger the flux linkage, the larger the power factor. As a result, LS-PMA-SynRM can improve the power factor and efficiency of electric motors compared with LS-SynRM.

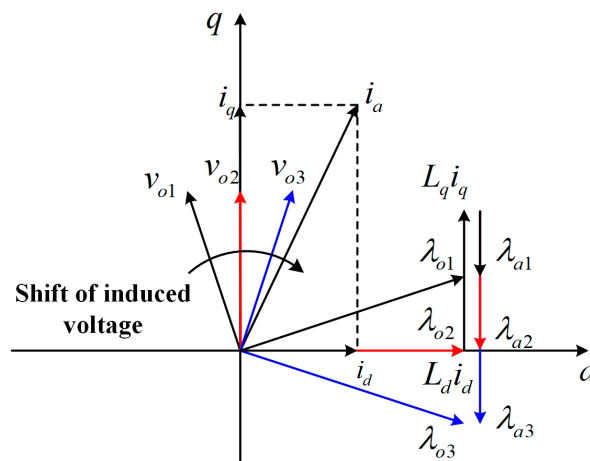


**Figure 2.** The vector diagram of LS-PMA-SynRM according to flux linkage by permanent magnet.

### 3. FEA Models of Reference Models

In this section, reference models (IM and LS-SynRM) are discussed in terms of specification and FEA model. In Section 3.1, the specification of reference models is introduced. In Section 3.2, the materials of motor are discussed for FEA. In Section 3.3, the performances of reference modes are analyzed by FEA.

#### 3.1. Specification of Reference Models

In order to compare the efficiency and power factor of LS-PMA-SynRM, the 5.5 kW 6-pole IM and LS-SynRM are selected as reference motors. Figure 3 shows the 2D FEA model of reference motors. The stators of IM and LS-SynRM have the same specification but the rotor is different. The number of squirrel-cage bars of the reference motors is the same, 42 bars. Therefore, considering the number of squirrel-cage bars, the number of barriers is designed to be three [8]. The detail specifications of the reference motors are shown in Table 1.

**Table 1.** Specification of reference models.

	Item	Value	Unit
Rated	Output Power	5.5	kW
	Input voltage	380	V
	Input frequency	60	Hz
Stator	Number of slots	54	–
	Stator outer diameter	220	mm
	Stator inner diameter	145	mm
Rotor	Number of slots	42	–
	Rotor outer diameter	144.2	mm
	Rotor inner diameter	42	mm
	Number of poles	6	–
	Stack length	170	mm
	Airgap length	0.3	mm
	Rib length	0.4	mm

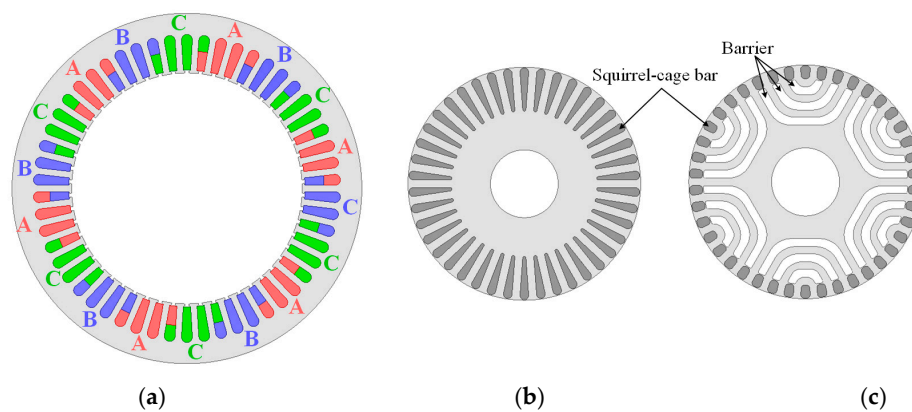


**Figure 3.** Reference models: (a) stator, (b) rotor of induction motor (IM), (c) rotor of LS-SynRM.

### 3.2. Material for FEA

Table 2 shows the material of the stator, rotor, winding, and the squirrel-cage bar. In industrial application, the cost of manufacture is the important factor because of price competitiveness. Considering the cost and core loss, 50PN470 (S18) has been mainly used as soft magnetic material of the stator and rotor in industrial applications. Figure 4 shows the B-H curve and core loss in 60 Hz of 50PN470. In general, the copper can improve the efficiency more than aluminum because of the high conductivity of copper as shown in Table 2. However, because the metal must be melted in the die-casting process, the aluminum with low melting point is mainly used as the material of die-casting. Therefore, considering the manufacture and copper loss, the material of winding and squirrel-cage bar is copper and aluminum, respectively.

**Table 2.** The material of each parts for finite element analysis (FEA).

Item	Material	Conductivity	Unit
Stator	50PN470 (S18)	$2.38 \times 10^6$	S/m
Rotor	50PN470 (S18)	$2.38 \times 10^6$	S/m
Winding	Copper	$5.8 \times 10^7$	S/m
Squirrel-cage bar	Aluminum	$3.6 \times 10^7$	S/m

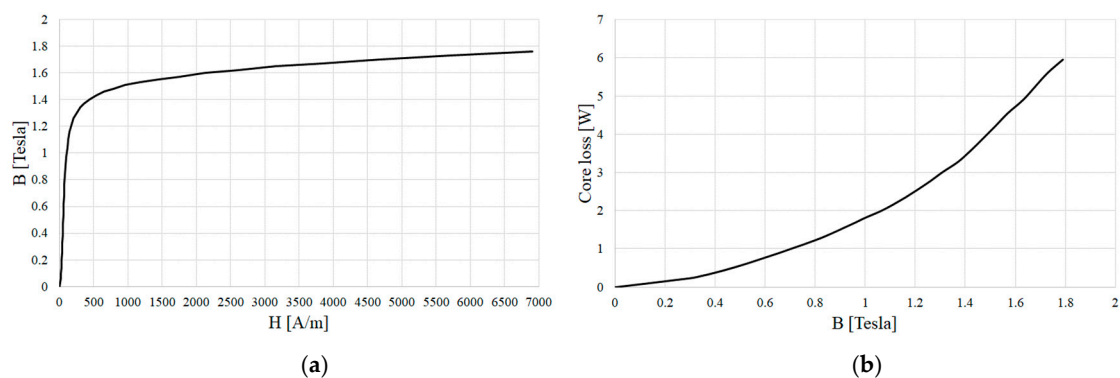


**Figure 4.** Characteristic of 35PN230: (a) B-H curve, (b) core loss.

### 3.3. FEA Result

To analyze the performance of the reference models, ANSYS MAXWELL 18.2 version was used. The time-step FEA was used to consider the mechanical and electromagnetic transient analysis [31,33]. Figure 5 shows the magnetic field density of the reference motors using FEA and Table 3 shows the characteristics of the reference motors. In Table 3, the core loss of IM is higher than that of LS-SynRM

because the magnetic flux density of IM is higher than that of LS-SynRM in Figure 5. Furthermore, IMs have a slip that represents the difference between the synchronous speed and the rotor speed. This slip induces an electromotive force in the squirrel-cage bar and generates the rotor copper loss that accounts for 31% of the total losses in Table 3. On other hand, for the stator copper loss, the current of LS-SynRM is higher than that of IM because the power factor is low under same output power and input voltage. As a result, the efficiency of IM is higher than that of LS-SynRM considering the total loss.

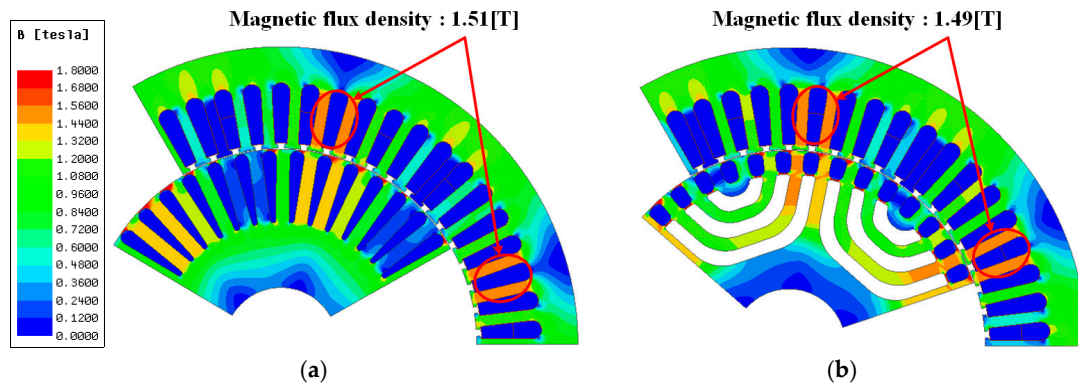


**Figure 5.** Electromagnetic analysis result of reference models: (a) IM, (b) LS-SynRM.

**Table 3.** Characteristics of reference models using FEA.

Item	Value		Unit
	IM	LS-SynRM	
Power	5.5	5.5	kW
Speed	1170.8	1200	rpm
Torque	48.1	45.5	Nm
Current	11.55	12.88	A
Core loss	94.36	90.12	W
Stator copper loss	214.35	266.69	W
Rotor copper loss	143.8	25.39	W
Total loss	452.55	382.21	W
Efficiency	91.46	92.46	%
Power factor	80.14	70.39	–

#### 4. Design of LS-PMA-SynRM

In this section, the performance of LS-PMA-SynRM is analyzed by FEA according to the position and length of permanent magnet. In Section 4.1, LS-PMA-SynRM is analyzed according to the position of magnet considering the manufacture. In Section 4.2, LS-PMA-SynRM is analyzed according to the length of the permanent magnet in the position obtained in Section 4.1.

To analyze the characteristics of LS-PMA-SynRM, the ferrite permanent magnet was inserted into the barriers of LS-SynRM. As LS-SynRM has the end-ring structure, as shown in Figure 6, the position of the magnet is limited. From Figure 6, the position magnet can be inserted into only first and second barriers. Therefore, the efficiency and power factor of LS-PMA-SynRM were analyzed considering the position of the magnet. Furthermore, the length of the magnet was designed to maximize the efficiency and power factor. Table 4 shows the ferrite permanent magnet data to analyze the LS-PMA-SynRM.

**Table 4.** Permanent magnet data.

Item	Value	Unit
Residual flux density	0.39	T
Coercive force	3.703	kOe

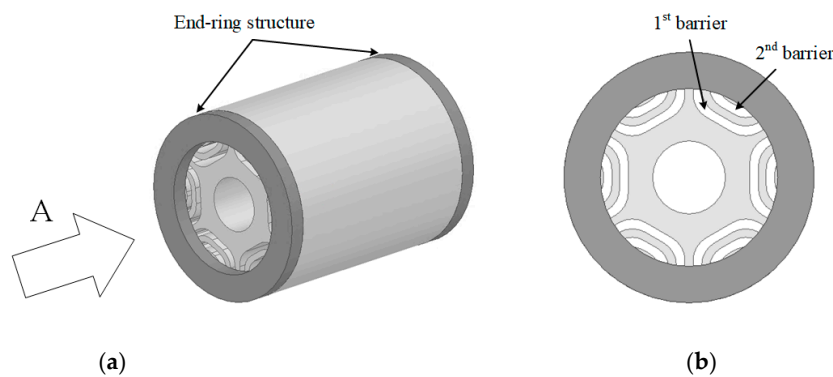


**Figure 6.** Rotor structure of LS-SynRM with end-ring (a) rotor and (b) view of A.

#### 4.1. Position of Magnet

Figure 7 shows the FEA models for analysis according to the position of the magnet. To analyze the characteristic of the LS-PMA-SynRM considering the position of the magnet, the length of the magnet is the same as 7 mm. Moreover, considering the end-ring structure, the position of the magnet is inserted into the first and second barrier. Figure 8 shows the magnetic flux density using FEA, and Figure 8 shows the loss analysis, efficiency, and power factor under the same output power conditions. In Figure 8, because the magnetic flux density of model 2 is larger than models 1 and 3, the core loss of model 2 is the larger in Figure 9. Figure 10 shows the magnetic flux density of air gap. As the magnetic flux density of model 3 is larger than other models, the efficiency and power factor are better, as shown in Figure 9b. Therefore, the model 3 was selected as the base model to analyze the characteristics of LS-PMA-SynRM according to the length of the magnet.

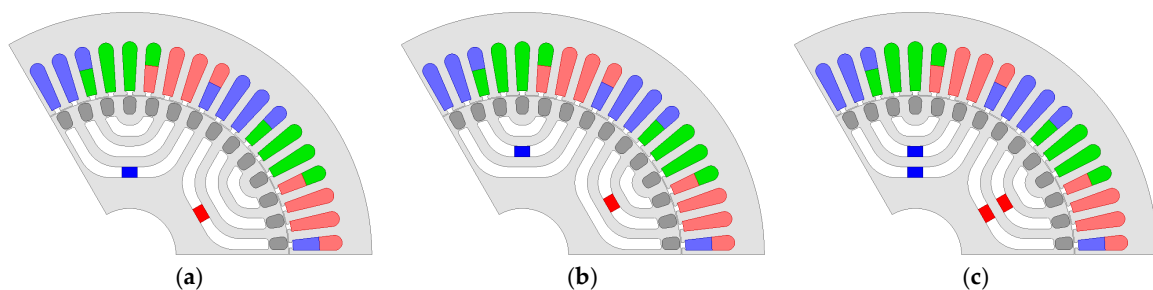


**Figure 7.** FEA model for analysis according to the position of magnet in (a) model 1, (b) model 2, and (c) model 3.

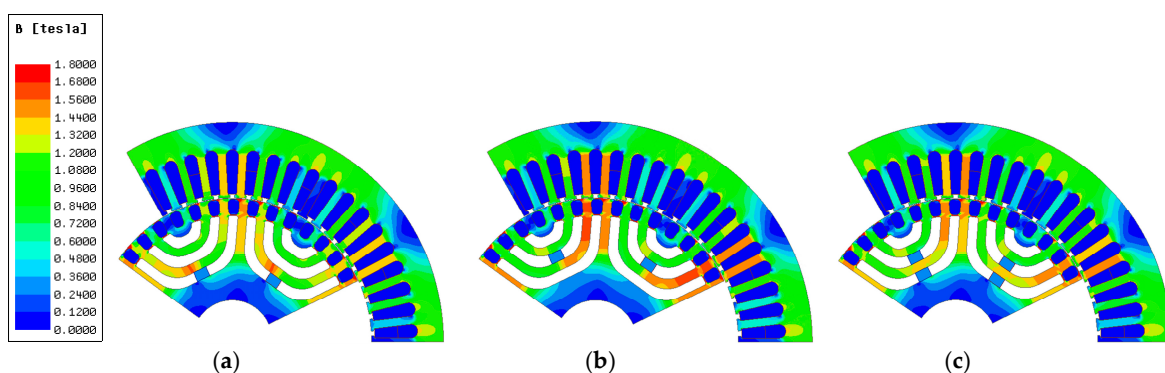


**Figure 8.** Electromagnetic analysis result using FEA according to the position of magnet in (a) model 1, (b) model 2, and (c) model 3.

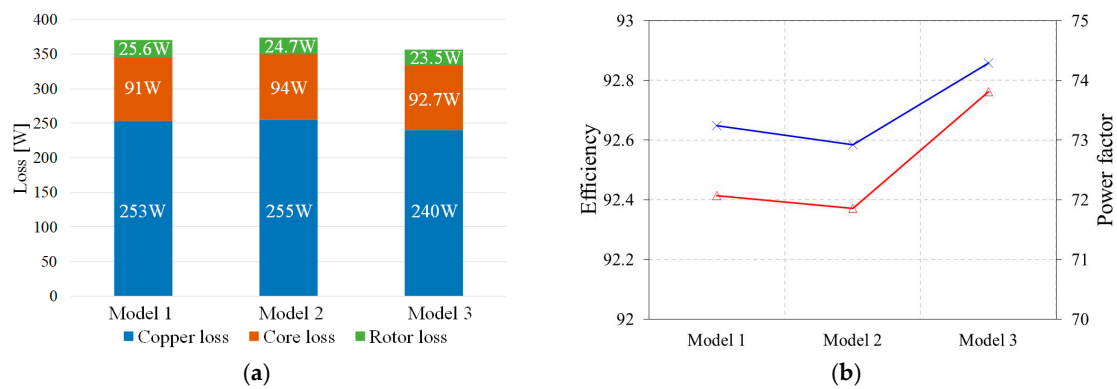


**Figure 9.** Electromagnetic analysis result using FEA according to the position of magnet: (a) loss, (b) efficiency and power factor.

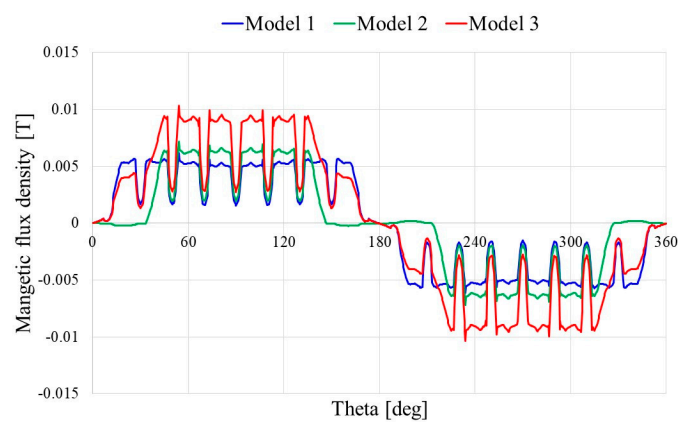


**Figure 10.** Magnetic flux density in air gap of analysis models.

#### 4.2. Length of Magnet

The characteristics of LS-PMA-SynRM were analyzed considering the length of the magnet. Figure 11 shows the design parameter of LS-PMA-SynRM. The lengths of the magnets of the first and second barriers are defined as  $W_{m1}$  and  $W_{m2}$ , respectively. Considering the length of the barriers and their manufacturer, the parameter ranges were selected. The length of the first magnet ranges from 1 to 17 mm and the length of second magnet from 0.5 to 8.5 mm. Figure 12 shows the FEA analysis result for parameters ( $W_{m1}$ ,  $W_{m2}$ ). The longer is the magnet, the higher the efficiency and power factor. Based on the FEA result, the final model was designed to maximize the efficiency and power factor.

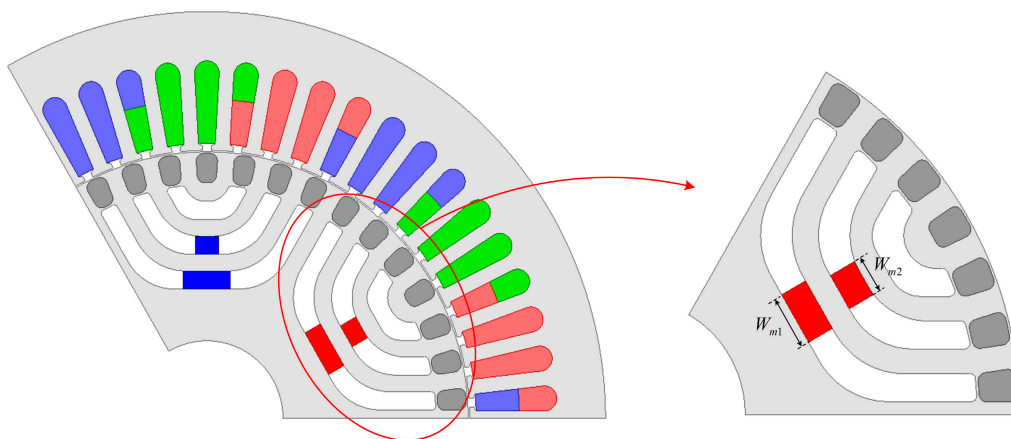


**Figure 11.** Parameter for analysis of the characteristic according to length of magnet.

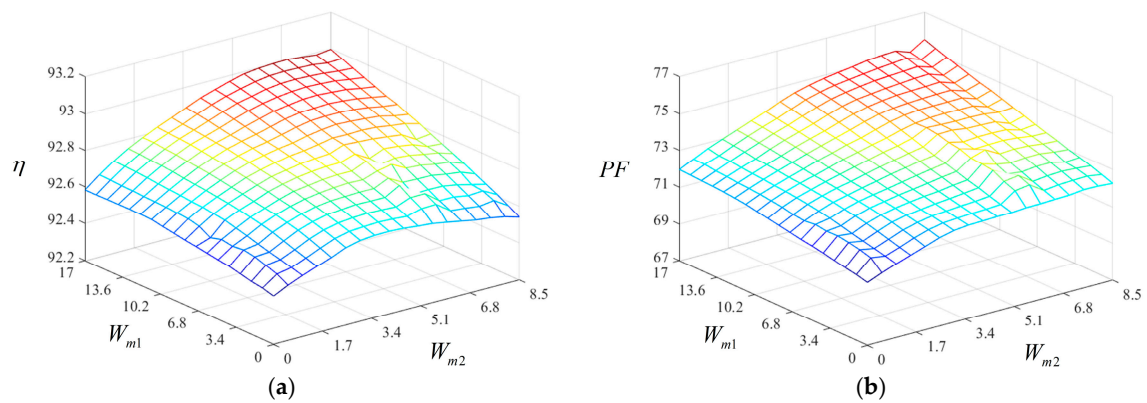


Figure 12. FEA analysis result according to length of magnet: (a) efficiency, (b) power factor.

### 4.3. Final Model of LS-PMA-SynRM

In Figure 12, considering the efficiency and power factor, the final model was designed so that the length of the first magnet was 17 mm and that of the second magnet was 8.5 mm. Figure 13a shows the final model of LS-PMA-SynRM and Figure 13b shows the magnetic flux density using FEA. Table 5 shows the FEA result for LS-PMA-SynRM. Compared with Table 3, the efficiency is improved by approximately 5.6% and the power factor is improved by approximately 5.2% compared with LS-SynRM. Based on the FEA result, the permanent magnet can be used to improve the efficiency and power factor based on the analysis result.

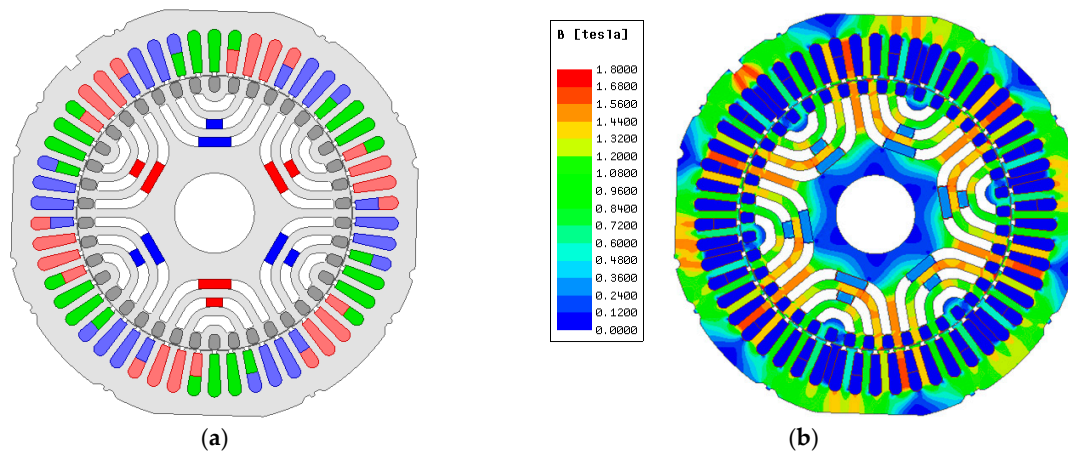


Figure 13. The final model of LS-PMA-SynRM: (a) FEA model, (b) magnetic flux density.

Table 5. FEA result of LS-PMA-SynRM.

Item	Value	Unit
Power	5.5	kW
Speed	1200	rpm
Torque	44	Nm
Current	11.98	A
Core loss	93.79	W
Stator copper loss	229.04	W
Rotor copper loss	24.84	W
Total loss	347.68	W
Efficiency	93	%
Power factor	75.5	–

## 5. Verification

The final models of LS-PMA-SynRM and reference model of IM were manufactured to verify the FEA result. In Section 5.1, the manufacture of LS-PMA-SynRM is discussed considering the die-casting process and permanent magnet. In Section 5.2, the experiments of IM and LS-PMA-SynRM are conducted and compared with FEA and experiment result according to load. In Section 5.3, the main advantages are discussed in comparison with previous literature.

### 5.1. Manufacture

Figure 14a,b shows the rotor and stator of the manufactured LS-PMA-SynRM. In Figure 14a, there is a bridge in the barrier as a support structure for the permanent magnet. In the die-casting process, the high pressures lead to aluminum leaking into the barriers. To prevent this problem, thin electrical steel sheets are placed on both ends of the rotor, as shown Figure 14c. Therefore, the electrical steel sheet is eliminated to insert the permanent magnet, as shown Figure 14d. When the die-casting is performed, the temperature is high, and this can lead to thermal demagnetization. Furthermore, because of the squirrel-cage bar slot, magnetization is difficult to attain. Therefore, the permanent magnet is assembled after magnetization.

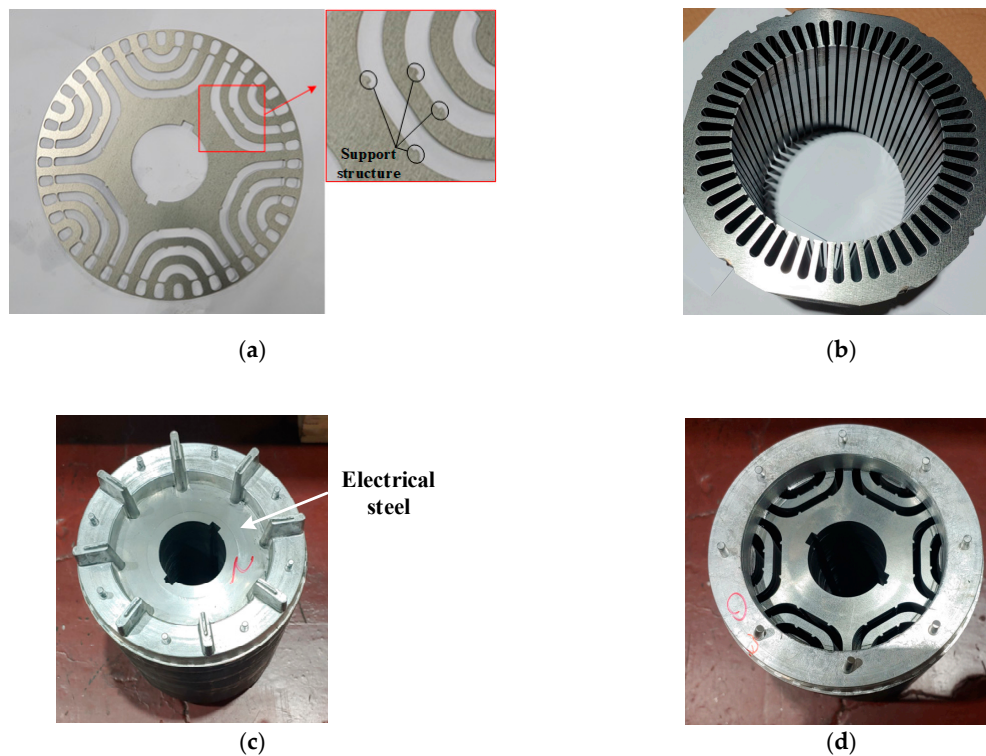


**Figure 14.** Manufacture LS-PMA-SynRM: (a) rotor core, (b) stator, (c) rotor before removing the electrical steel, and (d) rotor after removing the electrical steel.

### 5.2. Experiment Result

Experiments were conducted to verify the efficiency and power factor of IM and the final LS-PMA-SynRM. Figure 15 shows the dynamometer motor and experiment environment. The performance of the test motor was calculated using the power analyzer that is Yokogawa's WT1803E model. In addition, the temperature logger was used for the temperature saturation test. The temperature was measured through the temperature sensor and the measured temperature was recorded in the temperature logger as shown Figure 15. The dynamometer motor is the IM and allows the test motor to rotate at a synchronous speed. Through the V/f control, the dynamometer motor runs

up and reaches synchronous speed. The test motor is also operated at a synchronous speed and the voltage is applied to the test motor. The torque control is used to maintain the 5.5 kW output power in the dynamometer motor. The current sensor measures the current in the test motor, and the torque and speed are measured using the dynamometer motor. In the power analyzer, the input power, output power, efficiency, and power factor are calculated based on the measured voltage, current, torque, and speed. Figure 16 shows the efficiency of IM and LS-PMA-SynRM according to different loads. The performances of IM and LS-PMA-SynRM agree well with the results obtained from the FEA and experiments. Table 6 shows the experiment result of IM and LS-PMA-SynRM. Compared with the FEA result in Tables 3 and 5, the efficiency of IM and LS-PMA-SynRM is decreased by approximately 0.3% and the power factors are decreased by 6% and 4%, respectively.

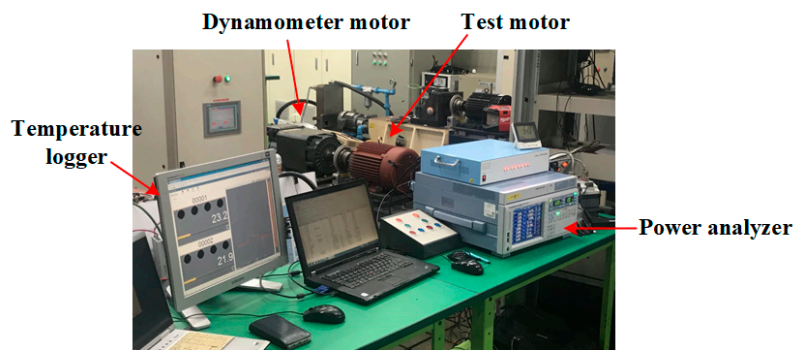


Figure 15. Experiment environment and test dynamometer.

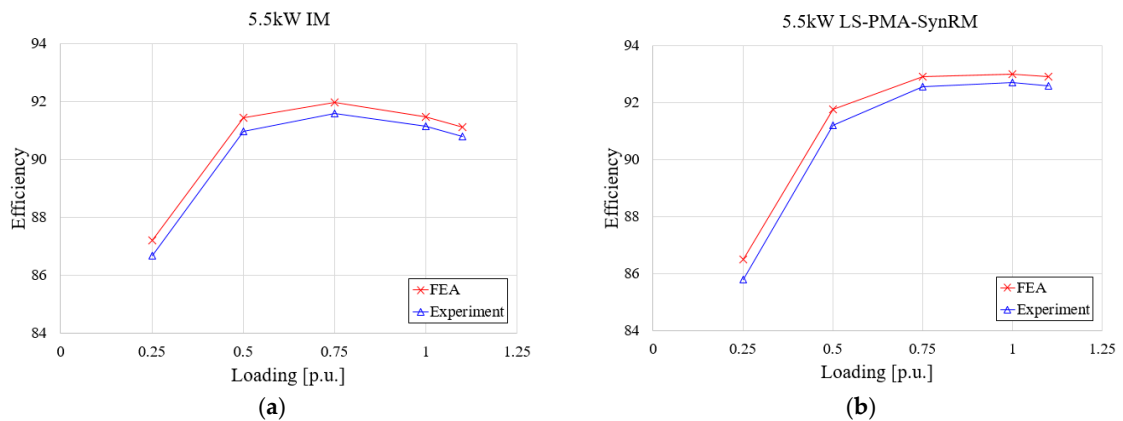


Figure 16. Experiment result of manufactured motors: (a) IM, (b) LS-PMA-SynRM.

Table 6. Experiment result of IM and LS-PMA-SynRM using the power analyzer.

Item	Value		Unit
	IM	LS-PMA-SynRM	
Power	5.5	5.5	kW
Speed	1175	1200	rpm
Torque	44.7	43.7	Nm
Current	12.3	12.6	A
Core loss	106	105.9	W
Stator copper loss	249.5	257.7	W
Rotor copper loss	124.6	0	W
Total loss	535.3	433.75	W
Efficiency	91.13	92.69	%
Power factor	74.5	71.2	–

### 5.3. Discussion

In previous literature, LS-SynRM have been studied as alternatives to IM due to high efficiency. However, because of the saliency characteristic of SynRM, LS-SynRM have a limited power factor. Referring to IEC 60034-1, not only the efficiency but also power factor is the important factor in industrial electrical machines. Therefore, the power factor of LS-SynRM must be improved to replace IM. In general, due to magnetic flux by permanent magnet, the power factor of PMA-SynRM is better than SynRM. However, because of the thermal demagnetization of ferrite magnet in the die-casting process, there is no research on LS-PMA-SynRM. This study discussed the design and analysis of LS-PMA-SynRM according to the position and length of permanent magnet considering the manufacture such as die-casting. In addition, the efficiency and power factor of LS-SynRM were verified by comparison with FEA and experiment. As a result, the efficiency and power factor were improved compared with LS-SynRM.

## 6. Conclusions

This study analyzed the efficiency and power factor of LS-PMA-SynRM considering the position and length of its permanent magnet. In addition, IM and LS-SynRM were analyzed to verify the performance of LS-PMA-SynRM under the condition of the same stator specification. Considering the die-casting and manufacturing processes, the permanent magnet was assembled after magnetization. Furthermore, the position of the permanent magnet was selected considering the end-ring. Further, considering this position, the performance of the LS-PMA-SynRM was analyzed and the base model was selected. Based on this model, the analysis parameter was selected, and the efficiency and power factor of electric motors was analyzed according to the length of the permanent magnet. The final model was designed using FEA. To verify the FEA result, LS-PMA-SynRM was manufactured and experiments were conducted. As a result, the FEA and experiment result of IM and LS-PMA-SynRM agree well, and the performance of LS-PMA-SynRM is improved compared with LS-SynRM. This study provided the design and manufacture of LS-PMA-SynRM as the alternative to IM. However, the power factor of LS-PMA-SynRM was still lower than IM. Therefore, the design of barrier, such as the length, angle, and thickness of barrier, must be optimized. In addition, the position and length of the permanent magnet according to design of barrier must be optimized to improve the efficiency and power factor. This requires further investigation about optimal design.

**Author Contributions:** H.K. conducted an analysis to improve the efficiency and power factor of electric motors. Y.P. investigated the research trend obtained using LS-SynRM. H.-C.L. reviewed the FEA result and guided this paper. P.-W.H. funded the research. J.L. verified and supervised the research. All authors have read and agreed to the published version of the manuscript.

**Funding:** This research was funded by the Energy Efficiency & Resources of the Korea Institute of Energy Technology Evaluation and Planning (KETEP) grant funded by the Korea government Ministry of Knowledge Economy (No. 2018201010633A) and in part by the Human Resources Program in Energy Technology of the Korea Institute of Energy Technology Evaluation and Planning (KETEP), granted financial resource from the Ministry of Trade, Industry & Energy, Republic of Korea (No. 20174030201750).

**Conflicts of Interest:** The authors declare no conflict of interest.

## References

1. Kersten, A.; Liu, Y.; Pehrman, D.; Thiringer, T. Rotor Design of Line-Start Synchronous Reluctance Machine with Round Bars. *IEEE Ind. Appl.* **2019**, *55*, 3685–3696. [[CrossRef](#)]
2. Almeida, A.T.D.; Ferreira, F.J.T.E.; Baoming, G. Beyond Induction Motors-Technology Trends to Move Up Efficiency. *IEEE Ind. Appl.* **2014**, *50*, 2103–2114. [[CrossRef](#)]
3. Almeida, A.T.D.; Ferreira, F.J.T.E.; Fong, J.A.C. Standards for Efficiency of Electric Motor. *IEEE Ind. Appl. Mag.* **2011**, *17*, 12–19. [[CrossRef](#)]
4. Matko, V.; Brezovec, B. Improved Data Center Energy Efficiency and Availability with Multilayer Node Event Processign. *Energies* **2018**, *11*, 2478. [[CrossRef](#)]

5. Jia, M.; Srinivasan, R.S.; Raheem, A.A. From occupancy to occupant behavior: An analytical survey of data acquisition technology, modeling methodologies and simulation coupling mechanisms for building energy efficiency. *Renew. Sustain. Energy Rev.* **2017**, *68*, 525–540. [[CrossRef](#)]
6. Ferreira, F.J.T.E.; Baoming, G.; Almeida, A.T.D. Reliability and Operation of High-Efficiency Induction Motors. *IEEE Ind. Appl.* **2016**, *52*, 4628–4637. [[CrossRef](#)]
7. Xie, Y.; Pi, C.; Li, Z. Study on Design and Vibration Reduction Optimization of High Starting Torque Induction Motor. *Energies* **2019**, *12*, 1263. [[CrossRef](#)]
8. Rafajdus, P.; Hrabovcova, V.; Lehocky, P.; Makys, P.; Holub, F. Effect of Saturation on Field Oriented Control of the New Designed Reluctance Synchronous Motor. *Energies* **2018**, *11*, 3223. [[CrossRef](#)]
9. Aguba, V.; Muteba, M.; Nicolae, D.V. Transient Analysis of a Start-up Synchronous Reluctance Motor with Symmetrical Distributed Rotor Cage Bars. In Proceedings of the 2017 IEEE AFRICON, Cape Town, South Africa, 18–20 September 2017.
10. Liu, H.C.; Lee, J. Optimum Design of an IE4 Line-Start Synchronous Reluctance Motor Considering Manufacturing Process Loss. *IEEE Trans. Ind. Electron.* **2018**, *65*, 3104–3114. [[CrossRef](#)]
11. Lee, J.K.; Jung, D.H.; Lim, J.; Lee, K.D.; Lee, J. A Study on the Synchronous Reluctance Motor Design for High Torque by Using RSM. *IEEE Trans. Magn.* **2018**, *54*, 8103005. [[CrossRef](#)]
12. Ozcelik, N.G.; Dogru, U.E.; Imeryuz, M.; Ergene, L.T. Synchronous Reluctance Motor vs. Induction Motor at Low-Power Industrial Applications: Design and Comparison. *Energies* **2019**, *12*, 2190. [[CrossRef](#)]
13. Tampio, J.; Kansakangas, T.; Suuriniemi, S.; Kolehmainen, J.; Kettunen, L.; Ikaheimo, J. Analysis of Direct-On-Line Synchronous Reluctance Machine Start-Up Using a Magnetic Field Decomposition. *IEEE Trans. Ind. Appl.* **2017**, *53*, 1852–1859. [[CrossRef](#)]
14. Boroujeni, S.T.; Bianchi, N.; Alberti, L. Fast Estimation of Line-Start Reluctance Machine Parameters by Finite Element Analysis. *IEEE Trans. Energy Convers.* **2011**, *26*, 1–8. [[CrossRef](#)]
15. Liu, H.C.; Hong, H.S.; Cho, S.; Lee, J.; Jin, C.S. Bubbles and Blisters Impact on Diecasting Cage to the Designs and Operations of Line-Start Synchronous Reluctance Motors. *IEEE Trans. Magn.* **2017**, *53*, 8202504. [[CrossRef](#)]
16. Zhao, W.; Xing, F.; Wang, X.; Lipo, T.A.; Kwon, B.-I. Design and Analysis of a Novel PM-Assisted Synchronous Reluctance Machine with Axially Integrated Magnets by the Finite-Element Method. *IEEE Trans. Magn.* **2017**, *53*, 8104104. [[CrossRef](#)]
17. Joo, K.-J.; Kim, I.-G.; Lee, J.; Go, S.-C. Robust Speed Sensorless Control to Estimated Error for PMA-SynRM. *IEEE Trans. Magn.* **2017**, *53*, 8102604. [[CrossRef](#)]
18. Kim, W.-H.; Kim, K.-S.; Kim, S.-J.; Kang, D.-W.; Go, S.-C.; Chun, Y.-D.; Lee, J. Optimal PM Design of PMA-SynRM for Wide Constant-Power Operation and Torque Ripple Reduction. *IEEE Trans. Magn.* **2009**, *45*, 4660–4663. [[CrossRef](#)]
19. Almeida, A.T.D.; Ferrera, F.J.T.E.; Duarte, A.Q. Technical and Economical Considerations on Super High-Efficiency Three-Phase Motors. *IEEE Trans. Ind. Appl.* **2014**, *50*, 1274–1285. [[CrossRef](#)]
20. Kong, Y.; Lin, M.; Yin, M.; Hau, L. Rotor Structure on Reducing Demagnetization of Magnet and Torque Ripple in a PMA-synRM With Ferrite Permanent Magnet. *IEEE Trans. Magn.* **2018**, *54*, 8108705. [[CrossRef](#)]
21. Mingardi, D.; Bianchi, N. Line-Start PM-Assisted Synchronous Motor Design, Optimization, and Tests. *IEEE Trans. Ind. Electron.* **2017**, *64*, 9739–9747. [[CrossRef](#)]
22. Jung, D.-H.; Kwak, Y.; Lee, J.; Jin, C.-S. Study on the Optimal Design of PMA-SynRM Loading Ratio for Achievement of Ultrapremium Efficiency. *IEEE Trans. Magn.* **2017**, *53*, 8001904. [[CrossRef](#)]
23. Liu, H.-C.; Joo, K.-J.; Oh, Y.J.; Lee, H.-J.; Seol, H.-S.; Jin, C.-S.; Kim, W.-H.; Lee, J. Optimal Design of an Ultra-Premium-Efficiency PMA-Synchronous Reluctance Motor with the Winding Method and Stator Parameters to Reduce Flu Leakage and Minimize Torque Pulsations. *IEEE Trans. Magn.* **2018**, *54*, 8207505. [[CrossRef](#)]
24. Wang, X.; Zhu, C.; Zhang, R.; Tang, R.; Song-Yop, H. Performance Analysis of Single-Phase Induction Motor Based on Voltage Source Complex Finite-Element Analysis. *IEEE Trans. Magn.* **2006**, *42*, 587–590. [[CrossRef](#)]
25. Lee, S.-H.; Kwon, S.; Lee, J.-J.; Hong, J.-P. Characteristic Analysis of Claw-Pole Machine Using Improved Equivalent Magnetic Circuit. *IEEE Trans. Magn.* **2009**, *45*, 4570–4573.
26. Shimotani, T.; Sato, T.; Igarashi, H. Fast Finite-Element Analysis of Motors Using Block Model Order Reduction. *IEEE Trans. Magn.* **2016**, *52*, 7207004. [[CrossRef](#)]

27. Lee, J.-J.; Lee, J.; Kim, K.-S. Design of a WFSM for an Electric Vehicle Based on a Nonlinear Magnetic Equivalent Circuit. *IEEE Trans. Appl. Supercond.* **2018**, *28*, 5206304. [[CrossRef](#)]
28. Lin, I.-H.; Hsieh, M.-F.; Kuo, H.-F.; Tsai, M.-C. Improved Accuracy for Performance Evaluation of Synchronous Reluctance Motor. *IEEE Trans. Magn.* **2015**, *51*, 8113404. [[CrossRef](#)]
29. Lee, B.-H.; Hong, J.-P.; Lee, J.-H. Optimum Design Criteria for Maximum Torque and Efficiency of a Line-Start Permanent-Magnet Motor Using Response Surface Methodology and Finite Element Method. *IEEE Trans. Magn.* **2012**, *48*, 863–866. [[CrossRef](#)]
30. Li, N.; Zhu, J.; Lin, M.; Yang, G.; Kong, Y.; Hau, L. Analysis of Axial Field Flux-Switching Memory Machines Based on 3-D Magnetic Equivalent Circuit Network Considering Magnetic Hysteresis. *IEEE Trans. Magn.* **2019**, *55*, 7203104. [[CrossRef](#)]
31. Zhang, Y.; Chau, K.T.; Zhang, D.; Liu, C. A Finite Element-Analytical Method for Electromagnetic Field Analysis of Electric Machines with Free Rotation. *IEEE Trans. Magn.* **2006**, *42*, 3392–3394. [[CrossRef](#)]
32. Sadiku, M.N.O. A Simple Introduction to Finite Element Analysis of Electromagnetic Problems. *IEEE Trans. Magn.* **1989**, *32*, 85–93. [[CrossRef](#)]
33. Liu, H.C.; Seol, H.S.; Kim, J.Y.; Lee, J. Design and Analysis of an IE4 Class Line-Start Synchronous Reluctance Motor Considering Total Loss and Starting Performance. *J. Electron. Mater.* **2019**, *48*, 1386–1394. [[CrossRef](#)]



© 2020 by the authors. Licensee MDPI, Basel, Switzerland. This article is an open access article distributed under the terms and conditions of the Creative Commons Attribution (CC BY) license (<http://creativecommons.org/licenses/by/4.0/>).